Hydrodynamic resistance of close-approached slip surfaces with a nanoasperity or an entrapped nanobubble

Tai-Hsi Fan[1] and Olga I. Vinogradova[1,2]
[1]*Max Planck Institute for Polymer Research, Ackermannweg 10, 55128 Mainz, Germany*
[2]*Laboratory of Physical Chemistry of Modified Surfaces, A.N.Frumkin Institute of Physical Chemistry and Electrochemistry, Russian Academy of Sciences, 31 Leninsky Prospect, 119991 Moscow, Russia*
(Received 27 July 2005; published 13 December 2005)

We present a general solution of hydrodynamic resistance of close-approached slippery surfaces with a nanoasperity or a nanobubble as an idealized roughness effect. Based on Reynolds' lubrication theory and a simple slip boundary condition, the pressure distribution in the thin liquid film is predicted analytically and the total hydrodynamic resistance force at limiting cases are formulated in terms of correction functions to the Taylor's equation. Accessible parameters are included for the drainage experiment using atomic force microscope or surface force apparatus. We provide case studies to demonstrate the implication of roughness effect and the possible uncertainties involved in the dynamic force measurement. We found that in the lubrication regime, the hydrodynamic resistance is dominated by the local behavior near the asperity, thus the apparent slip length can not always represent the surface roughness.

DOI: 10.1103/PhysRevE.72.066306 PACS number(s): 47.15.Gf, 68.08.−p, 68.15.+e

I. INTRODUCTION

The growing interest to fluid flow and mass transfer at nanoscale in confined geometries has introduced new research themes and questions to consider. Among them, the understanding of surface and interfacial phenomena such as wettability, slippage, roughness effect, elastic deformation, dispersion stability, and nanobubbles appeared on the flow and boundary has provided scientific foundation and opportunities to advance technologies including the manufacturing processes in food, pharmaceutical, biochemical, and semiconductor industries. An important issue well-recognized in the field of fluid science is that at the solid-liquid interface the classical no-slip condition does not always applicable [1], and in many cases it is necessary to correct the boundary condition with an amount of slippage relative to solid surface [2]. A simple hypothesis assumes that the slippery fluid element immediately in contact with the solid surface is resisted by the tangential traction f_t, which is proportional to the slip (tangential) velocity v_s. The proportional constant is defined as the friction coefficient β [1], expressed as $f_t=\beta v_s=\mu\partial v_s/\partial n$ where μ is dynamic viscosity and n is the surface normal directed into the liquid. It is also convenient to define the slip boundary condition using an apparent slip length b [2] as $v_s=b\partial v_s/\partial n$, where $b=\mu/\beta$. The proposition based on linear extrapolation of the velocity profile near the wall allows one to change the boundary condition from $b\to 0$ (no-slip) to $b\to\infty$ (no tangential stress) or to shift the wall position into the solid by a distance b so that one can accommodate the slippage by using a no-slip boundary condition in physical models.

At the atomic level, the slip length related to the fluid structure and the nonwetting surface have been theoretically simulated by molecular dynamics of Lennard-Jones (LJ) liquids [3–5]. A general nonlinear relationship between the slip and shear rate was established using LJ liquid for the Couette flow [4]. At the continuum level, it is commonly accepted that simple liquid do not slip on a smooth hydrophilic surface [6,7] except that the fluid flow is under a very high shear rate. Slip behavior can be caused by hydrophobicity, roughness, and the appearance of nanobubbles. For a smooth surface the best known example is the flow passing through a *hydrophobic* surface [8]. Such a slip was theoretically predicted [9,10] and experimentally measured [7,11,12], although on the experimental side the microphysics is less clear. It is commonly agreed that *roughness* of a hydrophilic surface causes viscous dissipation and leads to a no-slip condition [13]. Considerable theoretical efforts on fluid flow over a rough surface were focused on how to define an equivalent smooth surface. The mimetic roughness conditions range from an atomic level irregularity with various arrangement of surface atoms [14], microscopically randomly perturbed [15] or sparsely protruded surfaces [16], to the periodically arranged corrugated surface [17,18]. The fundamental importance of hydrodynamic interaction of rough particles related to the rheological properties of the particle suspension was carefully studied [19,20], where the sub-millimeter scale asperities generated were bonded to the large sphere by the sprinkling method or by rolling over the sand glass. However, a realistic formulation for a naturally rough surface is still formidable because of the uncertainties involved in complex hierarchical surface structure and nonuniform surface properties. Experimentally, situation seems to be not very clear. Thus, the apparent slip was recently reported for rough hydrophilic surfaces [21] Since the surface roughness can only increase viscous dissipation and the hydrodynamic resistance, it is naturally to suggest that the significant reduction in the viscous force interpreted in terms of apprarent slip reflects mostly the way of determination of the wall position. Indeed, the representative wall position can not be easily decoupled with the apparent slip length for either sparsely or densely, randomly or regularly packed asperities, at least for those experiments using atomic force microscope (AFM) and surface force apparatus (SFA). How-

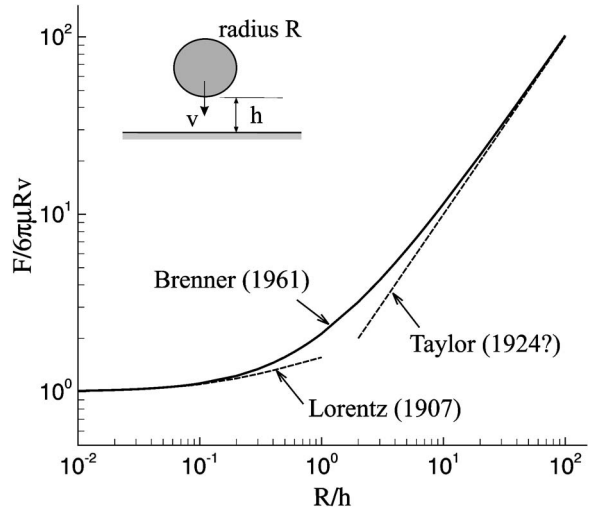

FIG. 1. Creeping flow resistance force for a spherical particle approaching toward a planar surface with no-slip boundary condition.

ever, as we will show below, just the idea of shifting the wall position is not sufficient to present surface roughness effect at least for the case with sparsely distributed asperities. Finally, slippage might also be a consequence of formation of *nanobubbles* [22]. The appearance of nanobubbles is closely related to cavitation, roughness [7,23] and hydrophobicity [22,24–27].

Early measurements for the slippery behavior were based on the change of flow rate or drag reduction as compared with those for the no-slip cases [28,29]. Direct measurement of the velocity profile adjacent to the slip surface is possible by using optical techniques such as total internal reflection and fluorescence recovering kinetics after photobleaching [30,31], particle image velocimetry [32,33], and double-focus fluorescence cross-correlation method [34]. A combining technique with optical trap and evanescent wave light scattering [35] may provide an alternative way to access the slip boundary condition. The so-called drainage method (see [6,7,36] for details) that allows measurement of the hydrodynamic resistance with high accuracy was used to deduce the correction function [37] compared with the Taylor's equation based on Reynolds' lubrication theory. Apparent slip length was determined by high speed force measurements using SFA [12,38] and AFM [7,21]. After Reynolds [39], the earliest literature related to drainage method is Lorentz's contribution in creeping flow for a spherical particle moving towards a plane wall [40]. The total resistance force F has been approximated by the singularity and image method at the limit of relatively large separation distance h compared to the particle radius R with approaching speed v (Fig. 1),

$$F = 6\pi\mu v R\left(1 + \frac{9}{8}\frac{R}{h+R}\right) \tag{1}$$

When the separation distance is relatively small or in the lubrication regime, one can evaluate the resistance force from the Taylor's equation for the case with no-slip boundary condition,

$$F = 6\pi\mu v R^2/h \tag{2}$$

The origins of this equation has been discussed [38] and concluded that Taylor solved this problem first although he never published the result, and the literature in 1924 often referred by the research community, does not exist. Perhaps it is because the derivation is straightforward from the Reynolds' approximation, researchers often consider Eq. (2) as an obvious result of Reynolds' lubrication theory. Brenner [41] laid out the exact solution

$$F = 6\pi\mu v R\lambda \tag{3}$$

where

$$\lambda = \frac{4}{3}\sinh(\alpha)\sum_{n=1}^{n=\infty}\frac{n(n+1)}{(2n-1)(2n+3)} \times\left(\frac{2\sinh[(2n+1)\alpha]+(2n+1)\sinh(2\alpha)}{4\sinh^2[(n+\frac{1}{2})\alpha]-(2n+1)^2\sinh^2(\alpha)}-1\right), \tag{4}$$

and $\alpha=\cosh^{-1}[(h+R)/R]$. His solution covers both limiting cases solved by Lorentz and Taylor (Fig. 1). When $R/h\to 0$, $\lambda\to 1$, the drag force approaches to the Stokes resistance law. As $R/h\to\infty$, $\lambda\to R/h$, the resistance force is consistent with the Taylor's equation. For slippery cases, Basset [42] has formulated a correction to the Stokes law ($R/h\to 0$),

$$F = 6\pi\mu v R\frac{\beta R+2\mu}{\beta R+3\mu} \tag{5}$$

where β is the friction coefficient. And in the lubrication regime ($R/h\to\infty$), Vinogradova [37] modified the Taylor's equation by a correction factor f^*,

$$F = \frac{6\pi\mu v R^2}{h}f^*, \quad f^* = \frac{h}{3b}\left[\left(1+\frac{h}{6b}\right)\ln\left(1+\frac{6b}{h}\right)-1\right] \tag{6}$$

where b is the slip length for both smooth surfaces and the correction factor f^* depends on the ratio h/b.

Our contribution in this paper focuses on formulating f^* for the surfaces covered by sparsely distributed asperities or nanobubbles. This arrangement is typical for a dynamic force measurement in the lubrication regime. Indeed, nanoasperities or nanobubbles are likely appeared at the surfaces that are considered to be molecularly smooth and could hardly be detected by AFM imaging [25,26]. Although it is difficult to tell which asperity or any asperity at the surface of AFM colloidal probe is actually near or in contact with the substrate, the flow field and pressure distribution can be understood by the simplified model with single asperity or a trapped nanobubble arranged along the center line. We found that the well-accepted idea of effective hydrodynamic surface roughness is not applicable for the limiting cases when the asperity is loosely packed, and the resistance force can be dominated by the local behavior around the small asperity. Thus a flow pasting through a rough surface is not always equivalent to a flow through a smooth surface with slippage.

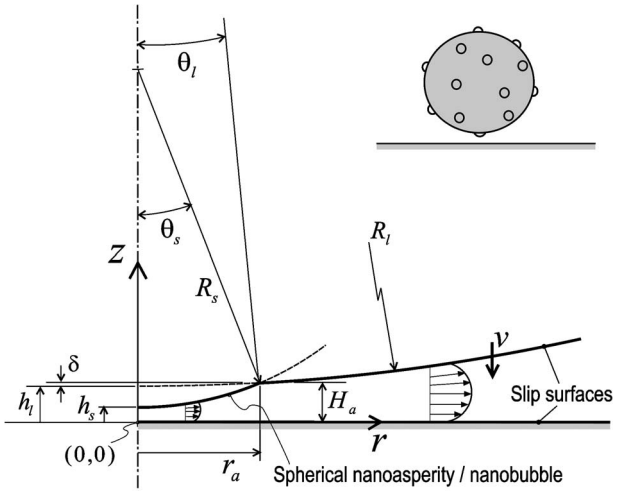

FIG. 2. Drainage of a thin liquid film confined between slip surfaces with an idealized roughness effect—a nanoasperity or an entrapped nanobubble protruded from the approaching surface.

We have reformulated the correction factor to the standard expression Eq. (6) to accommodate these effects.

II. ANALYSIS

Figure 2 shows the physical arrangement for the drainage analysis. We apply cylindrical coordinate system for the axisymmetric configuration with the radial coordinate axis **r** pointed outward, the axial coordinate axis **z** pointed upward, and the origin ($r=0$, $z=0$) affixed to the center point of the planar surface. The simplified roughness condition is represented by a symmetric asperity or an entrapped nanobubble with radius R_s protruded from the surface of the large spherical particle with radius R_l. Both spherical profiles have their center points located on the z axis. The solid sphere is moving toward the planar substrate with constant approaching speed v ($v>0$). The intersection point of the two spherical profiles is located at ($r=r_a$, $z=H_a$), and the dimensions h_l and h_s are the minimum separation distances between the extended large spherical profile and the asperity surface to the planar substrate, respectively. All hydrophobic surfaces are chemically similar with slip length b defined by $v_s=b\partial v_s/\partial n$. Parameters θ_l, θ_s, and δ are useful in finding h_l and R_s in practical measurements using AFM instrument with a colloidal particle attached to the cantilever. The model is developed for Newtonian fluid with low Reynolds number and relatively rigid surface/interface. We assume that the thin liquid film has thickness much smaller than the characteristic lengths of the small asperity, R_s, and the large particle, R_l, so that the hydrodynamic theory of lubrication [39] is applicable. In a simplified aqueous environment, we neglect electrical and molecular-level interactions between the slippery surfaces to facilitate the analytical solutions as a first step of further investigations.

A. Drainage flow with a spherical nanoasperity

Considering a spherical profile, $(z-R_l-h_l)^2+r^2=R_l^2$, the position of the upper boundary for the large sphere can be defined by the solution of the quadratic equation, $z=R_l+h_l-(R_l^2-r^2)^{1/2}$, and be approximated by the paraboloid of revolution, $z\sim h_l+r^2/2R_l$ [37]. Similarly, the paraboloid profile is used to describe the boundary of the protruded spherical asperity. Thus we can define the position of the upper boundary for the thin liquid film and separate it to the inner and outer regions in r direction: $z=h_s+r^2/2R_s$ for $0\leqslant r\leqslant r_a$ and $z=h_l+r^2/2R_l$ for $r_a\leqslant r<\infty$. For a low Reynolds number flow, the velocity field $\mathbf{v}=v_r\hat{\mathbf{e}}_r+v_z\hat{\mathbf{e}}_z$ satisfies the Stokes approximation, $\nabla p=\mu\nabla^2\mathbf{v}$, where p is the pressure field and μ is the dynamic viscosity. By further assuming that $h_s+r^2/2R_s\ll R_s$ and $h_l+r^2/2R_l\ll R_l$, the governing system based on the classical lubrication theory [39] in a cylindrical coordinate system is simplified to the r-momentum equation,

$$\frac{dp(r)}{dr}=\mu\frac{\partial^2 v_r(r,z)}{\partial z^2} \tag{7}$$

The z-momentum equation reduces to $\partial p/\partial z\sim 0$ and the pressure field is only a function of r. The continuity equation can be replaced by the integral form [43] for the drainage rate across the circumferential area of the thin liquid film, written as

$$\dot{Q}=2\pi r\int_0^{H(r)} v_r(r,z)dz=\pi r^2 v,\quad H(r)=h+\frac{r^2}{2R} \tag{8}$$

where v is the constant approaching speed of the particle (Fig. 2), and the upper limit of the integral is defined by $H(r)$ to simplify the notation here and for the following sections. Equations (7) and (8) are complemented by the velocity and pressure boundary conditions,

$$v_r=b\frac{\partial v_r}{\partial z}\ \text{at}\ z=0 \tag{9}$$

$$v_r\sim -b\frac{\partial v_r}{\partial z}\ \text{at}\ z=h+\frac{r^2}{2R} \tag{10}$$

$$p=0\ \text{as}\ r\to\infty \tag{11}$$

The governing system and the velocity boundary conditions above are applicable for both inner and outer regions of the thin liquid film. The exact solutions for the pressure and velocity fields are derived as follows.

1. Inner solution for $0\leqslant r\leqslant r_a$

The general solution of Eq. (7) is given by

$$v_r=\frac{1}{\mu}\frac{dp}{dr}\frac{z^2}{2}+Az+B \tag{12}$$

where the constants A and B are determined by the boundary conditions, Eqs. (9) and (10). By letting $H_s(r)=h_s+r^2/2R_s$, we have

$$A=-\frac{1}{2\mu}\frac{dp}{dr}H_s,\quad B=bA \tag{13}$$

and the solution v_r can be written as

$$v_r(r,z) = \frac{1}{2\mu}\frac{dp}{dr}[z^2 - (z+b)H_s] \tag{14}$$

Considering mass conservation, Eq. (8), we can substitute and integrate v_r to obtain the pressure gradient

$$\frac{dp}{dr} = -\mu v r\left[\frac{H_s^3}{6} + bH_s^2\right]^{-1} \tag{15}$$

Another approach to find the pressure gradient is to apply definite integration to the continuity equation, however, it requires extra boundary condition, $dp/dr=0$ at $r=0$, and a careful consideration of the Leibniz integral rule to eliminate the velocity component v_z at the slippery boundary [37]. Integrating Eq. (15) after transforming the dummy index from rdr to $R_s dH_s$, the pressure field is given by

$$p(r) = \frac{3\mu v R_s}{H_s^2}\left[\frac{H_s}{3b} - \frac{H_s^2}{18b^2}\ln\left(1 + \frac{6b}{H_s}\right)\right] + C \tag{16}$$

where the constant C is to be determined by the matched condition located at $r=r_a$.

2. Outer solution for $r_a \leqslant r < \infty$

Equations (7)–(13) are applicable for the solution in the outer region $r_a \leqslant r < \infty$ except that H_s is replaced by H_l where $H_l(r)=h_l+r^2/2R_l$. Similarly, the velocity field in the outer region is

$$v_r(r,z) = \frac{1}{2\mu}\frac{dp}{dr}[z^2 - (z+b)H_l] \tag{17}$$

And the pressure gradient becomes

$$\frac{dp}{dr} = -\mu v r\left[\frac{H_l^3}{6} + bH_l^2\right]^{-1} \tag{18}$$

The corresponding pressure field is given by

$$p(r) = \frac{3\mu v R_l}{H_l^2}\left[\frac{H_l}{3b} - \frac{H_l^2}{18b^2}\ln\left(1 + \frac{6b}{H_l}\right)\right] + D \tag{19}$$

where the constant D vanishes due to the far-field boundary condition defined by Eq. (11).

3. Matched solution

The unknown constant C in Eq. (16) can be determined by matching the pressure distributions, Eqs. (16) and (19) at the location $r=r_a$. We define the thickness of the thin liquid film at the matched point using notation H_a, where $H_a=H_l(r_a)=h_l+r_a^2/2R_l=H_s(r_a)=h_s+r_a^2/2R_s$, and the results are matched as

$$C = \frac{3\mu v(R_l - R_s)}{H_a^2}\left[\frac{H_a}{3b} - \frac{H_a^2}{18b^2}\ln\left(1 + \frac{6b}{H_a}\right)\right] \tag{20}$$

In summary, the pressure distributions are

$$p = \frac{3\mu v R_s}{H_s^2}p^*(H_s) + \frac{3\mu v(R_l - R_s)}{H_a^2}p^*(H_a) \tag{21}$$

for $0 \leqslant r \leqslant r_a$, and

$$p = \frac{3\mu v R_l}{H_l^2}p^*(H_l) \tag{22}$$

for $r_a \leqslant r < \infty$, where p^* is defined by the general form

$$p^*(H) = \frac{H}{3b} - \frac{H^2}{18b^2}\ln\left(1 + \frac{6b}{H}\right) \tag{23}$$

as a dimensionless correction function according to the solution developed for the close-approached spherical particles without roughness effect [37].

Since the total hydrodynamic force acting on the solid sphere is dominated by the pressure force, $dF \sim p(r)2\pi r dr$. Transforming the dummy index from rdr to RdH we can integrate Eqs. (21) and (22) over their corresponding domains to obtain the total force acting on the particle,

$$F = 2\pi\left(\int_{h_s}^{H_a} p(r)R_s dH_s + \int_{H_a}^{\infty} p(r)R_l dH_l\right) \tag{24}$$

After simplification, the final result can be expressed by

$$F = \frac{6\pi\mu v R_l^2}{h_l}f^* \tag{25}$$

where f^* is the dimensionless correction function for the total resistance force, and we obtain

$$\begin{aligned} f^* = {} & \frac{h_l}{3b}\left(\frac{R_s}{R_l}\right)^2\left[\left(1 + \frac{h_s}{6b}\right)\ln\left(1 + \frac{6b}{h_s}\right)\right. \\ & \left. - \left(1 + \frac{H_a}{6b}\right)\ln\left(1 + \frac{6b}{H_a}\right)\right] + \frac{h_l}{R_l}\left(\frac{r_a}{H_a}\right)^2\left(1 - \frac{R_s}{R_l}\right)\left[\frac{H_a}{6b}\right. \\ & \left. - \frac{H_a^2}{36b^2}\ln\left(1 + \frac{6b}{H_a}\right)\right] \\ & + \frac{h_l}{3b}\left[\left(1 + \frac{H_a}{6b}\right)\ln\left(1 + \frac{6b}{H_a}\right) - 1\right] \end{aligned} \tag{26}$$

Note that both velocity field and the pressure gradient can also be matched at $r=r_a$.

4. Asymptote for small b

To simplify Eq. (26), we look for an asymptote for the case with small slip length b. Indeed, when $b \ll O(h_s) \sim O(h_l) \sim O(H_a)$, Eq. (26) can be expanded to

$$\begin{aligned} f^* = {} & \left(\frac{R_s}{R_l}\right)^2\frac{1}{3\epsilon_2}[1 + 3\epsilon_1 - 6\epsilon_1^2 + \cdots - (1 + 3\epsilon_3 - 6\epsilon_3^2 + \cdots)] \\ & + \frac{h_l}{R_l}\left(\frac{r_a}{H_a}\right)^2\left(1 - \frac{R_s}{R_l}\right)(1/2 - 2\epsilon_3 + 9\epsilon_3^2 + \cdots) + \frac{1}{3\epsilon_2}(3\epsilon_3 \\ & - 6\epsilon_3^2 + \cdots) \end{aligned} \tag{27}$$

where the small parameters $\epsilon_1 \sim \epsilon_3$ are defined by

$$\epsilon_1 = b/h_s, \quad \epsilon_2 = b/h_l, \quad \epsilon_3 = b/H_a \tag{28}$$

Since $(\epsilon_1 - \epsilon_3)/\epsilon_2 = r_a^2 h_l/(2R_s h_s H_a)$, and $\epsilon_3/\epsilon_2 = h_l/H_a$, the leading order approximation for Eq. (27) gives a simple form,

$$f^* \sim \frac{r_a^2 h_l}{2R_s h_s H_a}\left(\frac{R_s}{R_l}\right)^2 + \frac{h_l}{2R_l}\left(\frac{r_a}{H_a}\right)^2\left(1-\frac{R_s}{R_l}\right) + \frac{h_l}{H_a} \quad (29)$$

The leading behavior, Eq. (29), is the exact solution for the case with no-slip boundary condition, $b=0$. Similarly, by considering $b \ll O(H_s) \sim O(H_a) \sim O(H_l)$, and letting $\epsilon = b/H$, the correction function for the pressure field Eq. (23) can be approximated by

$$p^* = 1 - 4\epsilon + 18\epsilon^2 + \cdots . \quad (30)$$

Thus the pressure fields for the case with no-slip boundary condition are given by Eqs. (21) and (22) with the leading effect of the pressure correction function, $p^*=1$. And the velocity fields are simply given by Eqs. (14) and (17) with $b=0$.

For the extreme case with $b \to \infty$, or $\partial v_r/\partial z \to 0$ at both boundaries, this approach will generate a physically unreasonable result when the correction functions p^* [Eq. (23)] and f^* [Eq. (26)] both approach to zero. This misleading result is because the second-order derivative term $\partial^2 v_r/\partial z^2$ vanishes in the governing Stokes equation, for that the established lubrication model [Eq. (7)] based on this dominated viscous term is no longer a valid approximation.

5. Limiting cases with large and small asperities

In the limiting cases with a very large asperity, $R_s \to R_l$, $r_a \to \infty$, we can replace R_s by R, h_s by h, and H_s by H to recover the result derived for the slippery surface without roughness effect [37]. That is, the pressure fields in Eqs. (21)–(23) approach to

$$p = \frac{3\mu v R}{H^2} p^*, \quad p^* = \frac{H}{3b} - \frac{H^2}{18b^2}\ln\left(1+\frac{6b}{H}\right) \quad (31)$$

for $0 \leqslant r < \infty$, and the hydrodynamic resistance force given by Eqs. (25) and (26) approaches to Eq. (6).

In the limiting case with a very small asperity, $R_s \to 0$, $r_a \to 0$, $H_a \to h_l \sim h_s$, we can replace R_l by R, h_l by h, and H_l by H to recover the identical results given by Eqs. (31) and (6). When no-slip condition is further applied to these limiting cases with very large and very small asperities, Eqs. (29) and (30) comply with the Taylor's equation where $f^*=1$ and $p^*=1$.

B. Drainage flow with a nanobubble

We further consider the drainage flow with an undeformable gas bubble entrapped by a surface cavity. This assumption is justified provided the maximum hydrodynamic pressure located at the center position is at least an order of magnitude smaller than the pressure inside the nanobubble.

1. Inner and outer solutions

The assumptions made for Sec. II A are also applicable when replacing the spherical asperity by a nanobubble. Thus the governing system does not change except that the velocity boundary condition, Eq. (10) is replaced by a free surface condition with vanished shear stress for $0 \leqslant r \leqslant r_a$,

$$\frac{\partial v_r}{\partial z} \sim 0 \text{ at } z = H_s = h_s + \frac{r^2}{2R_s} \quad (32)$$

The corresponding inner velocity field is

$$v_r(r,z) = \frac{1}{2\mu}\frac{dp}{dr}[z^2 - 2(z+b)H_s] \quad (33)$$

From mass conservation principle, the corresponding pressure gradient becomes

$$\frac{dp}{dr} = -\mu v r\left[\frac{2}{3}H_s^3 + 2bH_s^2\right]^{-1} \quad (34)$$

Thus

$$p(r) = \frac{3\mu v R_s}{H_s^2}\left[\frac{H_s}{6b} - \frac{H_s^2}{18b^2}\ln\left(1+\frac{3b}{H_s}\right)\right] + C \quad (35)$$

for $0 \leqslant r \leqslant r_a$, and the constant C is to be determined by the matched condition. The outer solutions for $r_a \leqslant r < \infty$ are not repeated since they are exactly the same as those presented in Sec. II A 2.

2. Matched solution

At the transition region where $r=r_a$ and $H_s=H_l=H_a$, the inner pressure field is determined by matching Eq. (35) and the equivalent outer form, Eq. (19). The constant C is then given by

$$C = \frac{\mu v}{bH_a}\left(R_l - \frac{R_s}{2}\right) + \frac{\mu v}{6b^2}\left[R_s \ln\left(1+\frac{3b}{H_a}\right) - R_l \ln\left(1+\frac{6b}{H_a}\right)\right] \quad (36)$$

In summary, the pressure distributions are

$$p = \frac{3\mu v R_s}{H_s^2} p^* + C, \quad p^* = \frac{H_s}{6b} - \frac{H_s^2}{18b^2}\ln\left(1+\frac{3b}{H_s}\right) \quad (37)$$

for $0 \leqslant r \leqslant r_a$, and

$$p = \frac{3\mu v R_l}{H_l^2} p^*, \quad p^* = \frac{H_l}{3b} - \frac{H_l^2}{18b^2}\ln\left(1+\frac{6b}{H_l}\right) \quad (38)$$

for $r_a \leqslant r < \infty$. The total force acting on the particle carrying the nanobubble can also be expressed by $F = (6\pi\mu v R_l^2/h_l) f^*$ where the new modification function is

$$\begin{aligned} f^* = {} & \frac{h_l}{6b}\left(\frac{R_s}{R_l}\right)^2 \\ & \times\left[\left(1+\frac{h_s}{3b}\right)\ln\left(1+\frac{3b}{h_s}\right) - \left(1+\frac{H_a}{3b}\right)\ln\left(1+\frac{3b}{H_a}\right)\right] \\ & + \frac{h_l}{6R_l}\left(\frac{r_a}{H_a}\right)^2\frac{H_a}{b}\left(1-\frac{R_s}{2R_l}\right) - \frac{h_l}{36R_l}\left(\frac{r_a}{H_a}\right)^2\frac{H_a^2}{b^2} \\ & \times\left[\ln\left(1+\frac{6b}{H_a}\right) - \frac{R_s}{R_l}\ln\left(1+\frac{3b}{H_a}\right)\right] \\ & + \frac{h_l}{3b}\left[\left(1+\frac{H_a}{6b}\right)\ln\left(1+\frac{6b}{H_a}\right) - 1\right] \end{aligned} \quad (39)$$

Note that only the pressure fields can be matched at $r=r_a$. The velocity fields and the pressure gradients have jump conditions located at the matched point. This result suggests there exists an overlapping region where the flow is in transition from fully slip to partially slip conditions. For a very low Reynolds number flow, this undefined region is limited to a very short distance as compared with the separation distance H_a, thus the lubrication theory is not applicable in this region. We assume this transition length is negligible to avoid the complexity in solving full Stokes equation, and this issue does not affect the result for total resistance force since the pressure distribution is continuous.

3. Asymptote for small b

In the case of small slippage, $b \ll O(h_s) \sim O(h_l) \sim O(H_a)$, Eq. (39) can be expanded by the small parameters ϵ_1, ϵ_2, and ϵ_3 as listed in Eq. (28),

$$f^* = \left(\frac{R_s}{R_l}\right)^2 \frac{1}{6\epsilon_2}\left[1+\frac{3}{2}\epsilon_1-\frac{3}{2}\epsilon_1^2+\cdots - \left(1+\frac{3}{2}\epsilon_3-\frac{3}{2}\epsilon_3^2+\cdots\right)\right] + \frac{h_l}{R_l}\left(\frac{r_a}{H_a}\right)^2\left(1-\frac{R_s}{2R_l}\right)\frac{1}{6\epsilon_3} - \frac{h_l}{R_l}\left(\frac{r_a}{H_a}\right)^2 \frac{1}{36\epsilon_3^2}\left[6\epsilon_3-18\epsilon_3^2+72\epsilon_3^3+\cdots - \frac{R_s}{R_l}\left(3\epsilon_3-\frac{9}{2}\epsilon_3^2+9\epsilon_3^3+\cdots\right)\right] + \frac{1}{3\epsilon_2}(3\epsilon_3-6\epsilon_3^2+\cdots) \tag{40}$$

Replacing $(\epsilon_1-\epsilon_3)/\epsilon_2$ by $r_a^2 h_l/(2R_s h_s H_a)$, and ϵ_3/ϵ_2 by h_l/H_a, the leading order approximation of Eq. (40) gives

$$f^* \sim \frac{h_l r_a^2}{8 h_s H_a R_s}\left(\frac{R_s}{R_l}\right)^2 + \frac{h_l}{2R_l}\left(\frac{r_a}{H_a}\right)^2\left(1-\frac{R_s}{4R_l}\right)+\frac{h_l}{H_a} \tag{41}$$

This leading behavior is the exact solution for the case with no-slip condition ($b=0$) at solid boundaries with a trapped nanobubble. Similarly, for $b \ll O(H_s) \sim O(H_a) \sim O(H_l)$, the constant C in Eq. (36) can be simplified,

$$C = \frac{\mu v}{bH_a}(R_l - R_s/2) + \frac{\mu v}{6b^2}[R_s(3\epsilon_3 - 9\epsilon_3^2/2+\cdots) - R_l(6\epsilon_3-18\epsilon_3^2+\cdots)] = \frac{\mu v}{6b^2}(-9R_s/2+18R_l)\epsilon_3^2+\cdots \sim \frac{3\mu v R_l}{H_a^2}\left(1-\frac{R_s}{4R_l}\right)+O(\epsilon_3) \tag{42}$$

The correction functions for pressure distributions, Eqs. (37) and (38), are approximated by

$$p^* = \frac{1}{4}-\frac{1}{2}\epsilon_1+\cdots \tag{43}$$

for $0 \leqslant r \leqslant r_a$, and

$$p^* = 1-4\epsilon_2+\cdots \tag{44}$$

for $r_a \leqslant r < \infty$ where the small parameters are redefined by $\epsilon_1 = b/H_s$, $\epsilon_2 = b/H_l$, and $\epsilon_3 = b/H_a$.

For no-slip case, the pressure fields are given by the leading terms of Eqs. (42)–(44) with $C = 3\mu v R_l(1-R_s/4R_l)/H_a^2$, $p^* = 1/4$ for $0 \leqslant r \leqslant r_a$, and $p^* = 1$ for $r_a \leqslant r < \infty$, and the velocity fields are conformed with Eq. (33) as the inner solution and Eq. (17) as outer solution with $b=0$.

4. Limiting cases with a small bubble

We further conclude the analytical solutions for four limiting cases with undeformable nanobubbles and large solid boundaries as follows.

(a) *A very small bubble and large solid boundaries with finite slip length b*. In this limiting case, $R_s \to 0$, $r_a \to 0$, $H_a \to h_l$, we can replace R_l by R, h_l by h, and H_l by H in Eq. (38) for the pressure field, Eq. (39) for the total force, to recover consistent solutions to those derived for a slippery surface without roughness effect [37], as already defined in Eqs. (31) and (6).

(b) *A very small bubble and large solid boundaries with* $b=0$. When no-slip condition is applied to this limiting case for $0 \leqslant r < \infty$, Eqs. (41) and (44) can be further reduced to $f^*=1$ and $p^*=1$, thus the resistance force is consistent with the Taylor's equation.

(c) *A single nanobubble approaching to the substrate with finite b*. Without the mixed boundary condition for the upper surface, the constant C vanishes as we define $p \to 0$ as $r \to \infty$ using Eq. (37). We can replace R_s by R and H_s by H for the pressure field in Eq. (37) and recover the solution derived for an infinitesimally slippery surface approaching to a substrate with a finite slip length b [37], given by

$$p = \frac{3\mu v R}{H^2} p^*, \quad p^* = \frac{H}{6b} - \frac{H^2}{18b^2}\ln\left(1+\frac{3b}{H}\right) \tag{45}$$

for $0 \leqslant r < \infty$. And direct integration of above equation gives

$$F = \frac{6\pi\mu v R^2}{h} f^*, \quad f^* = \frac{h}{6b}\left[\left(1+\frac{h}{3b}\right)\ln\left(1+\frac{3b}{h}\right)-1\right] \tag{46}$$

(d) *A single nanobubble approaching to the substrate with* $b=0$. When $b \ll O(h) \leqslant O(H)$ as an extreme condition in case (c), the leading order approximation of Eqs. (45) and (46) lead to the exact solution when $b=0$,

$$p^* = \frac{1}{4}, \quad f^* = \frac{1}{4} \tag{47}$$

III. RESULTS AND DISCUSSION

Based on the final expressions derived, we illustrate case studies specifically designed for the ongoing AFM measurements using a colloidal particle attached to the cantilever. All results are in dimensional forms to facilitate the physical interpretation. The pressure field and resistance force are determined by three key factors: (i) The slip length, (ii) the particle/substrate separation distance, and (iii) the appearance of asperities/bubbles in various sizes, and their combination effects. We skip the linear effects due to the dynamic viscosity and the particle approaching speed since both pa-

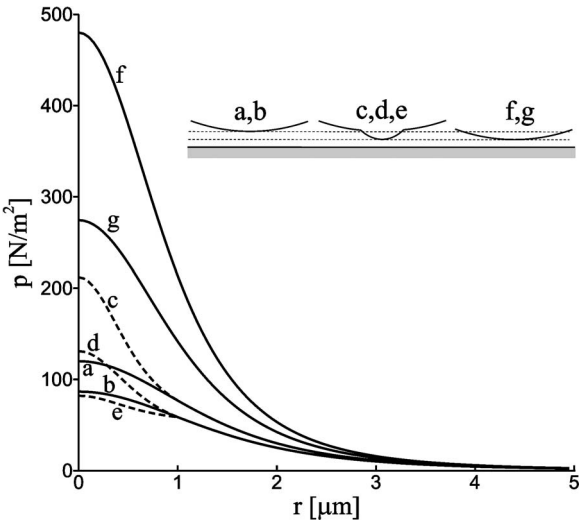

FIG. 3. The comparison of instantaneous pressure fields induced by close-approached surfaces with $\mu=10^{-3}$ kg/ms, $v=20$ μm/s, $R_l=20$ μm, and $b=10$ nm. The detail boundary conditions and additional geometry parameters are (a, no-slip; b, slip) $h_l=100$ nm, (c, no-slip/asperity; d, slip/asperity; e, slip/bubble) $h_s=50$ nm, $h_l\sim 100$ nm, $r_a=1.0$ μm, $h_a=125$ nm, and $R_s\sim 6.7$ μm, (f, no-slip; g, slip) $h_l=50$ nm.

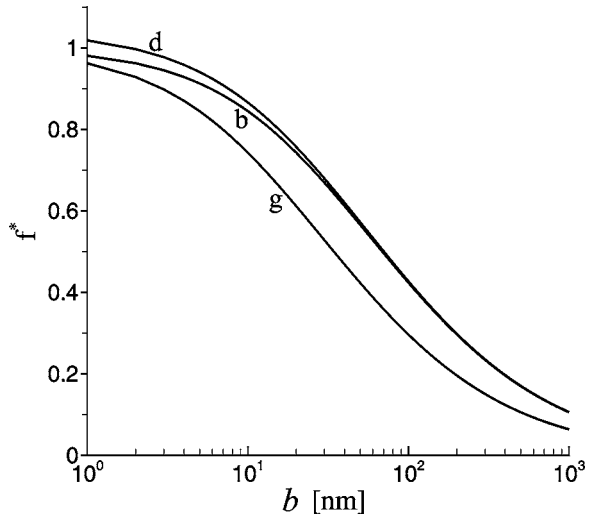

FIG. 4. Correction function f^* vs slip length b corresponding to the configurations and separation distances of cases b, d, and g in Fig. 3.

rameters are factored out from the correction functions, and we assume that they have fixed values $\mu=0.001$ kg/ms and $v=20$ μm/s. In a typical AFM experiment in evaluating the slip length, one can determine the measurable parameters R_l, h_s, H_a, and r_a by direct surface profiling using conventional AFM probe. Because the radius and center point of the idealized asperity are unknowns, these parameters are required to determine h_l and R_s from simple geometry relations (Fig. 2),

$$h_l = H_a - \zeta, \quad \zeta = R_l(1-\cos\theta_l), \quad \theta_l = \sin^{-1}(r_a/R_l) \quad (48)$$

and

$$R_s = \left(\frac{r_a}{\sin\theta_s}\right), \quad \theta_s = \pi - 2\phi, \quad \phi = \tan^{-1}\left(\frac{r_a}{H_a - h_S}\right) \quad (49)$$

Figure 3 shows the results of instantaneous pressure fields in a various combination of the key effects aforementioned. To facilitate the interpretation, we use rather large asperity/bubble in cases c, d, and e for comparison. The particle radius and the approaching speed are remained fixed at $R_l=20$ μm and $v=20$ μm/s. All cases studied have vanishing pressure at $r\geqslant 5$ μm compared with the magnitude of the concentrated pressure near the center point. Cases a, c, and f with no-slip boundary condition express higher pressure distributed along the radial direction compared with the results obtained by the corresponding slip cases b, d, and g. Observing the perfectly smooth particle in case a and its identical case f, case f has closer particle/substrate separation distance reducing from 100 to 50 nm. Its pressure field increases exactly four folds, which verifies the inverse square effect of the separation distance for the no-slip case with $p^*=1$ and $p=3\mu vR/H^2$. Cases c and d (dashed lines) have protruded microasperity and their pressure distributions fall into the range between two groups (a,b) and (f,g), however, the concentrated pressure only raises from the intersection point of two spherical profiles toward the axial line, $0<r\leqslant r_a$, in contrast to the effective range $0\leqslant r<\infty$ for the slip effect. This is a direct result of the identical far-field boundary condition assigned to the pressure equation for both cases with and without asperities. In the case e, we include a microbubble and show that the buildup of pressure field near the center point is relatively low compared to all other cases due to the finite slip length and the free surface boundary condition at the solid and bubble surfaces, respectively.

Figure 4 illustrates the slip length effect to the force correction function f^*. Cases b ($h_l=100$ nm) and g ($h_l=50$ nm) are the results from Eq. (6) for a smooth surface, and case d ($h_s=50$ nm) is the result of Eq. (26) for a surface with a protruded asperity. About fifty percent of the resistance force is significantly reduced when $O(b)\sim O(h)\sim O(50\text{ nm})$ compared with no-slip case. By comparing cases b and g, the force reduction becomes more significant as the separation distance decreases. When an asperity appears (case d), the correction function can reach slightly beyond unity near the no-slip regime because the base case for comparison is formulated by the distance h_l in the Taylor's equation instead of the true separation distance h_s. Comparing cases b and d, the configurational effect that causes higher pressure distribution near the asperity vanishes as the slip length increases.

Figure 5 shows the approach curves of cases $a-e$ corresponding to those cases demonstrated in Fig. 3. The approach curve depicts the total resistance force contributed by the local pressure force vs the minimum particle/substrate separation distance. The particle approaches from 600 nm away from the substrate down to 20 nm where the classical no-slip case (a) monotonically increases its maximum resistance up to 7.5 nN. This peak value reduces significantly to 4.3 nN when slip length 10 nm is applied, shown by case b.

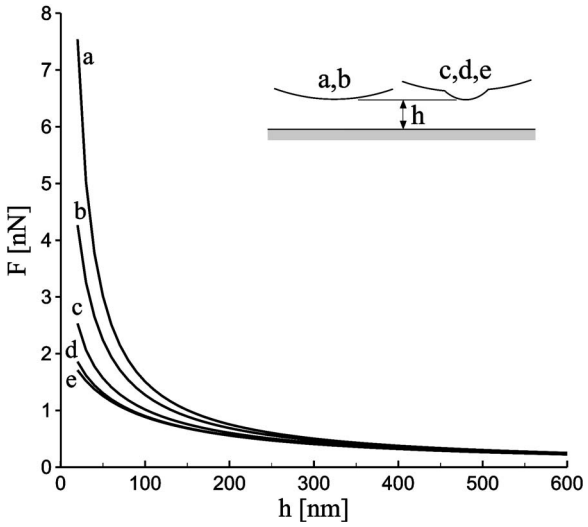

FIG. 5. Approach curves showing total resistance force vs minimum separation distance corresponding to cases $a-e$ in Fig. 3.

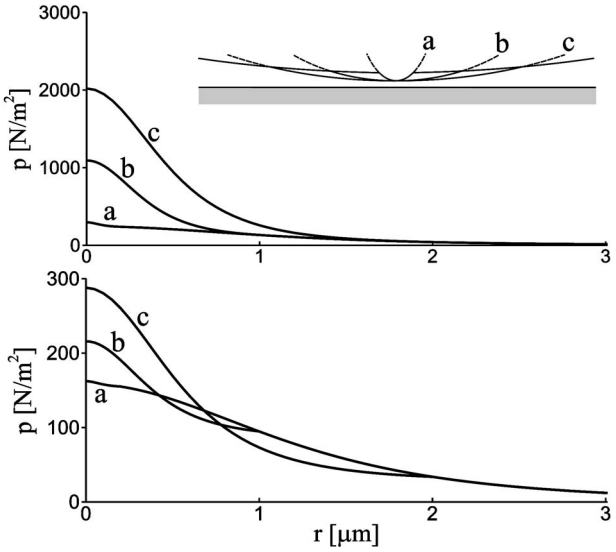

FIG. 6. Instantaneous pressure fields for various sizes of asperities (upper section, $b=0$) and bubbles (lower section, $b=10$ nm on solid surfaces) with $\mu=10^{-3}$ kg/ms, $v=20$ μm/s, $R_l=20$ μm, $h_s=20$ nm, $h_l\sim 70$ nm. Additional parameters have the following values: (a) $r_a=200$ nm, $H_a=71$ nm, $R_s\sim 418$ nm, (b) $r_a=1$ μm, $H_a=95$ nm, $R_s\sim 6.7$ μm, (c) $r_a=2$ μm, $H_a=170$ nm, $R_s\sim 13.4$ μm.

Comparing no-slip cases a and c, the resistance force reduces in case c because the pressure is relieved around the asperity and continuously decreases as being away from the center point. For slip case d and e, the resistance force drops further to values less than 2 nN due to the effect combining slip and pressure relief. Evidently for AFM experiments in predicting the slip length, if a simple roughness pattern appears, one should not ignore the effect generated by asperities or bubbles, otherwise the slip length will be overpredicted since both slip and the existence of asperity provide pressure relief and correspondingly reduce the total resistance force. For example, if we increase the slip length from 10 to 30 nm for case b, its approach curve will be hardly distinguished from the one obtained by curve c, where no-slip conditions is applied and an asperity is protruded about 50 nm from the profile of the large sphere.

In AFM/SFA experiments the size effect can be excluded by a pre-profiling experiment using an AFM probe. Quantitative comparisons in Figs. 6 and 7 show that the deviation of pressure fields (Fig. 6) can be clearly seen from cases a and b in the upper section presenting asperities, and cases a and b in the lower section for bubbles, but is not very distinguishable for the approach curves predicted in Fig. 7. The deviation of the resistance force from cases a to b is not obvious even in the near-field regime with separation distance less than 50 nm (Fig. 7). This is because higher pressure only building up near the very center region with relative small fraction of the surface area, and its integral force contribution is negligible compared to the total resistance. In case c, the deviation becomes significant when the asperity/bubble size increases to $R_s\sim 13.4$ μm.

IV. CONCLUSIONS

We present exact and approximate solutions for various cases of hydrodynamic resistance force of close-approached smooth and rough surfaces. The idealized roughness effect is presented by a single asperity or an entrapped bubble that occupies only a small surface area of the colloidal probe. The asperities or bubbles are assumed sparsely distributed so that the analytical solution can be obtained for an axisymmetric case under the lubrication regime. Our analysis is in particular suitable for AFM/SFA experiments in determining constant slip length by fitting the approach curves. The results indicate: (i) For a simple rough surface, that is, a surface without periodic or hierarchical structure, one should not apply a position shift for the solid boundary as an apparent wall position to accommodate the deviation from those for a per-

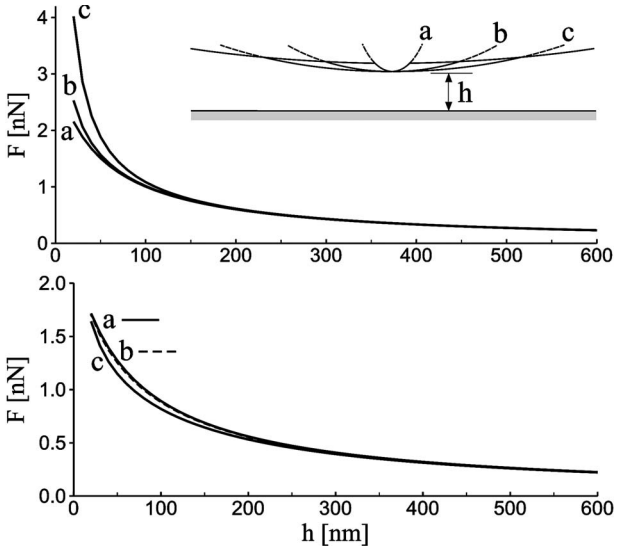

FIG. 7. Approach curves showing total resistance force vs minimum separation distance for cases a, b, and c corresponding to the upper and lower sections demonstrated in Fig. 6.

fectly smooth surface. The pressure buildup is a local effect and its value strongly depends on the size and shape of the single protruded asperity/bubble. (ii) The slip behavior due to the physicochemical properties of the solid surface or the aqueous environment is often convoluted with the roughness effect. For example, one can change the slip length to match the pressure distribution, thus the experimental data need to be considered carefully in case of an accidental fit that leads to misinterpretations. Finally, we have provided physical parameters that can be used as a starting point to evaluate a simple roughness effect combined with slippery boundary conditions using AFM/SFA measurement techniques. Potential analysis including far/near-field physicochemical effects such as electric double layer and van der Waals forces may also be considered under this framework.

ACKNOWLEDGMENT

This work was partly supported by a DFG priority program "Micro and Nanofluidics" (Vi 243/1-1).

[1] H. Lamb, *Hydrodynamics* (Dover, New York, 1932).
[2] P. G. de Gennes, Rev. Mod. Phys. **57**, 827 (1985).
[3] P. A. Thompson and M. O. Robbins, Phys. Rev. A **41**, 6830 (1990).
[4] P. A. Thompson and S. M. Troian, Nature (London) **389**, 360 (1997).
[5] J.-L. Barrat and L. Bocquet, Phys. Rev. Lett. **82**, 4671 (1999).
[6] D. Y. C. Chan and R. G. Horn, J. Chem. Phys. **83**, 5311 (1985).
[7] O. I. Vinogradova and G. E. Yakubov, Langmuir **19**, 1227 (2003).
[8] O. I. Vinogradova, Int. J. Min. Process. **56**, 31 (1999).
[9] L. Bocquet and J.-L. Barrat, Phys. Rev. E **49**, 3079 (1994).
[10] D. Andrienko, B. Dünweg, and O. I. Vinogradova, J. Chem. Phys. **119**, 13106 (2003).
[11] C. Cottin-Bizonne, B. Cross, A. Steinberger, and E. Charlaix, Phys. Rev. Lett. **94**, 056102 (2005).
[12] J. Baudry, E. Charlaix, A. Tonck, and D. Mazuyer, Langmuir **17**, 5232 (2001).
[13] S. Richardson, J. Fluid Mech. **59**, 707 (1973).
[14] T. M. Galea and P. Attard, Langmuir **20**, 3477 (2004).
[15] K. M. Jansons, Phys. Fluids **31**, 15 (1988).
[16] K. Sarkar and A. Prosperetti, J. Fluid Mech. **316**, 223 (1996).
[17] L. M. Hocking, J. Fluid Mech. **76**, 801 (1976).
[18] N. Lecoq, R. Anthore, B. Cichocki, P. Szymczak, and F. Feuillebois, J. Fluid Mech. **513**, 247 (2004).
[19] J. R. Smart and D. T. Leighton, Phys. Fluids A **1**, 52 (1989).
[20] Y. Zhao and R. H. Davis, J. Fluid Mech. **492**, 101 (2003).
[21] E. Bonaccurso, H.-J. Butt, and V. S. J. Craig, Phys. Rev. Lett. **90**, 144501 (2003).
[22] O. I. Vinogradova, N. F. Bunkin, N. V. Churaev, O. A. Kiseleva, A. V. Lobeyev, and B. W. Ninham, J. Colloid Interface Sci. **173**, 443 (1995).
[23] C. Cottin-Bizonne, J. L. Barrat, L. Bocquet, and E. Charlaix, Nat. Mater. **2**, 237 (2003).
[24] N. Ishida, M. Sakamoto, M. Miyahara, and K. Higashitani, Langmuir **16**, 5681 (2000).
[25] G. E. Yakubov, H.-J. Butt, and O. I. Vinogradova, J. Phys. Chem. B **104**, 3407 (2000).
[26] O. I. Vinogradova, G. E. Yakubov, and H.-J. Butt, J. Chem. Phys. **114**, 8124 (2001).
[27] P. Attard, Adv. Colloid Interface Sci. **104**, 75 (2003).
[28] N. V. Churaev, V. D. Sobolev, and A. N. Somov, J. Colloid Interface Sci. **97**, 574 (1984).
[29] K. Watanabe, Yanuar, and H. Udagawa, J. Fluid Mech. **381**, 225 (1999).
[30] R. Pit, H. Hervet, and L. Leger, Phys. Rev. Lett. **85**, 980 (2000).
[31] T. Schmatko, H. Hervet, and L. Leger, Phys. Rev. Lett. **94**, 244501 (2005).
[32] D. C. Tretheway and C. D. Meinhart, Phys. Fluids **14**, L9 (2002).
[33] P. Joseph and P. Tabeling, Phys. Rev. E **71**, 035303 (2005).
[34] D. Lumma, A. Best, A. Gansen, F. Feuillebois, J. O. Rädler, and O. I. Vinogradova, Phys. Rev. E **67**, 056313 (2003).
[35] A. R. Clapp and R. B. Dickinson, Langmuir **17**, 2182 (2001).
[36] O. I. Vinogradova, Langmuir **14**, 2827 (1998).
[37] O. I. Vinogradova, Langmuir **11**, 2213 (1995).
[38] R. G. Horn, O. I. Vinogradova, M. E. Mackay, and N. Phan-Thien, J. Chem. Phys. **112**, 6424 (2000).
[39] O. Reynolds, Philos. Trans. R. Soc. London **177**, 157 (1886).
[40] H. A. Lorentz, Abhand. Theor. Phys. Leipzig **1**, 23 (1907).
[41] H. Brenner, Chem. Eng. Sci. **16**, 242 (1961).
[42] A. B. Basset, *A Treatise on Hydrodynamics, Vol. 2* (Dover, New York, 1961).
[43] H. Schlichting, *Boundary Layer Theory* (McGraw-Hill, New York, 1979).